

# From Sequential to Spatial: Reordering Autoregression for Efficient Visual Generation

Siyang Wang<sup>1</sup> Hanting Li<sup>2</sup> Wei Li<sup>2</sup> Jie Hu<sup>2</sup> Xinghao Chen<sup>2</sup> Feng Zhao<sup>1</sup>

<sup>1</sup>University of Science and Technology of China

<sup>2</sup>Huawei Noah’s Ark Lab

{lihanting3,wei.lee,hujie23,xinghao}@huawei.com

siyangw@mail.ustc.edu.cn, fzha0956@ustc.edu.cn

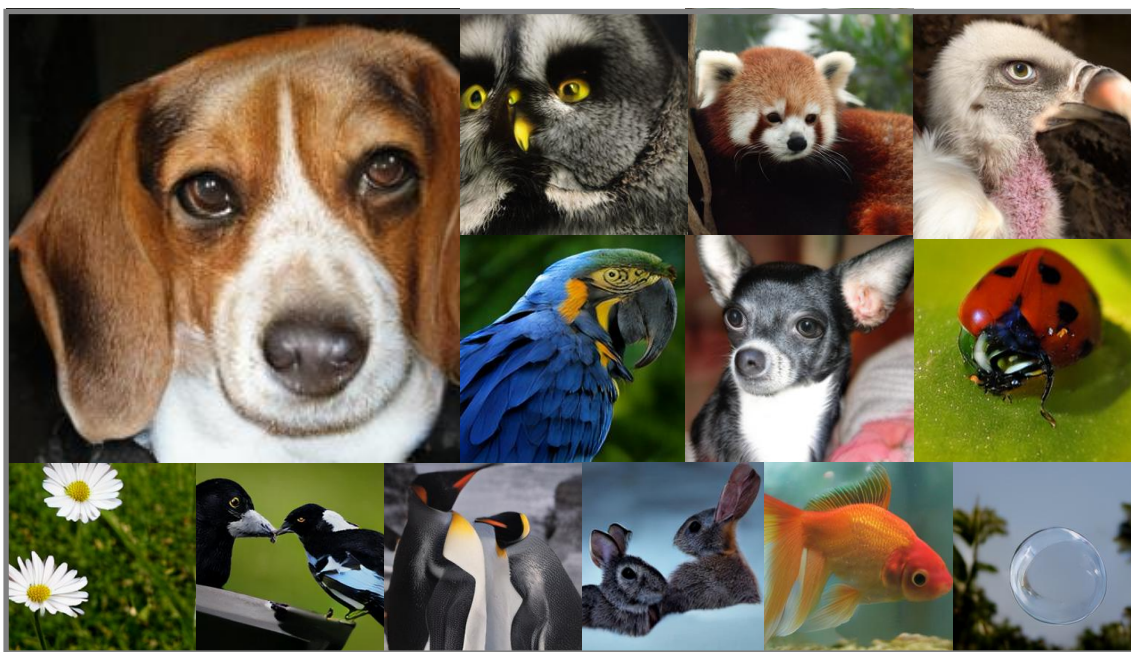


Figure 1. Generated samples from RadAR-XL. We show samples at different aspect ratios (top) and zero-shot image editing results (bottom) including class-conditional editing and out-painting . Please zoom in for details.

## Abstract

Inspired by the remarkable success of autoregressive models in language modeling, this paradigm has been widely adopted in visual generation. However, the sequential token-by-token decoding mechanism inherent in traditional autoregressive models leads to low inference efficiency. In this paper, we propose RadAR, an efficient and parallelizable framework designed to accelerate autoregressive visual generation while preserving its representational capacity. Our approach is motivated by the observation that visual tokens exhibit strong local dependencies and spatial correlations with their neighbors—a property not fully ex-

ploited in standard raster-scan decoding orders. Specifically, we organize the generation process around a radial topology: an initial token is selected as the starting point, and all other tokens are systematically grouped into multiple concentric rings according to their spatial distances from this center. Generation then proceeds in a ring-wise manner, from inner to outer regions, enabling the parallel prediction of all tokens within the same ring. This design not only preserves the structural locality and spatial coherence of visual scenes but also substantially increases parallelizability. Furthermore, to address the risk of inconsistent predictions arising from simultaneous token generation with limited context, we introduce a nested attention mecha-

*nism. This mechanism dynamically refines implausible outputs during the forward pass, thereby mitigating error accumulation and preventing model collapse. By integrating radial parallel prediction with dynamic output correction, RadAR reduces the number of inference steps from 256 to only 13, achieving up to a 5.6× speedup on the ImageNet dataset and significantly improving generation efficiency.*

## 1. Introduction

Autoregressive (AR) models demonstrate remarkable performance in language modeling [3, 10, 19, 42] and exhibit considerable potential for the development of artificial general intelligence. To extend the success of AR models from language to visual domain, researchers [11, 26] begin to explore the application of AR models in image generation. Pioneering works such as VQVAE-2 [27] and Parti [44] establish the fundamental feasibility of autoregressive visual generation by discretizing images into sequences of visual tokens, with subsequent research efforts [31, 32, 41] progressively pushing the performance boundaries. These models not only achieve visual fidelity comparable to or surpassing contemporary state-of-the-art diffusion models but, more significantly, provide architectural foundations for unified multimodal understanding and generation. This progress enables the development of integrated models capable of processing text, images, and video within a unified framework. However, these performance improvements come with considerable computational demands. In conventional autoregressive approaches for visual generation, two-dimensional images are typically flattened into one-dimensional sequences following raster-scan order and processed through sequential token prediction. This sequential processing mechanism establishes a quadratic relationship between the number of required inference steps and the image resolution, imposing significant constraints on generation efficiency. Consequently, deploying autoregressive models in practical scenarios faces substantial challenges, with generation speed becoming a major bottleneck hindering their widespread application, especially in scenarios requiring high-throughput requirements.

To address these efficiency limitations, the research community develops various methods for accelerating sequence generation. Existing methods generally fall into two primary categories. The first category attempts to break the strict sequential constraints of conventional autoregressive generation by allowing parallel prediction of multiple image tokens in a single inference step. The representative work MaskGIT [6] innovatively integrates masked modeling strategies with non-autoregressive generation, achieving significant acceleration by iteratively predicting and refining tokens at multiple masked positions. Similarly, PAR [39] further explores the potential of parallel decoding

within random positions or block-constrained regions. Nevertheless, these methods still face limitations in the trade-off between generation quality and efficiency. The second category seeks breakthroughs from the perspective of feature representation. Works represented by VAR [33] introduce multi-scale token representations, achieving an order-of-magnitude reduction in generation steps. However, this multi-scale token representation fundamentally differs in architecture from the universal flat token representation (e.g., CLIP [25, 46], DINO [5, 21]), preventing direct utilization of general visual representations learned from large-scale vision-language pairs. This compatibility issue severely restricts the interoperability of such methods with modern multimodal systems [34, 40, 47], impeding their broad application in complex systems requiring collaboration with existing perceptual backbones.

To systematically investigate more efficient visual decoding mechanisms, this paper conducts an in-depth analysis of the attention distribution patterns in autoregressive visual models. Our analysis reveals that visual content inherently exhibits strong locality. As shown in Fig. 2, although LlamaGen [31] is forced to follow the raster-scan sequence order during training, its attention distribution strongly reflects the inherent two-dimensional spatial structure of visual content. Specifically, when processing the current token, LlamaGen allocates significant attention weights not only to temporally adjacent tokens in the sequence but also to tokens that are temporally distant yet spatially proximate in the original image structure. This observation emphasizes the importance of modeling two-dimensional spatial relationships directly, beyond linear sequences. The conventional raster-scan order imposes a one-dimensional constraint that conflict with natural visual structure, forcing the model to learn to compensate for this structural mismatch during training, ultimately degrading both generation efficiency and semantic consistency.

Building on the above insights, we propose RadAR—a radial parallel autoregressive generative framework designed to maintain full representational capacity while achieving efficient inference. The framework establishes an initial token as the radial center and systematically partitions remaining tokens into concentric rings based on spatial distance. The generation process progresses ring by ring radially from the inside out, with all tokens within the same ring decoded in parallel. This design significantly enhances parallelism while preserving the locality and spatial coherence of visual structures. However, parallel generation introduces critical challenges: when multiple tokens are decoded simultaneously without sufficient contextual constraints, semantically inconsistent predictions are prone to occur. To address this, we further design a nested attention mechanism that operates at both inter-ring and intra-ring levels. By iteratively refining unreasonable outputs, this

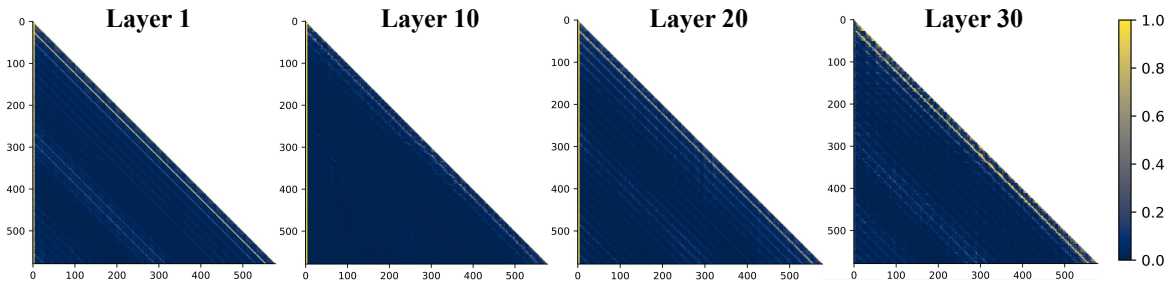


Figure 2. The distribution of attention scores across visual tokens in different layers of the LlamaGen-XL [31]. Slash lines indicate that significant attention scores are allocated to tokens at fixed intervals, corresponding to tokens in the same column of previous rows.

mechanism effectively suppresses error propagation and enhances generation robustness.

Experimental results demonstrate that by integrating radial parallel prediction with dynamic output correction, RadAR effectively addresses the speed limitations inherent in traditional autoregressive models. The proposed framework achieves a speedup of up to 5.6× on the ImageNet dataset, offering a scalable and high-performance solution for next-generation visual content synthesis.

## 2. Related Work

### 2.1. Autoregression in Language Modeling.

The autoregressive modeling paradigm first emerges in the field of natural language processing (NLP) [3, 24, 37, 38, 48], with the core idea of generating sequences by predicting each element in a sequence based on the previous elements through conditional probabilities. However, this simple mechanism has demonstrated remarkable scalability across multiple dimensions. On one hand, it follows an observable and reproducible scaling law, where every leap in computing power, parameters, and data volume brings predictable performance gains. On the other hand, once the scale of parameters exceeds a critical threshold, the model suddenly emerges with zero-shot and few-shot generalization capabilities. Without fine-tuning for specific tasks, it can be applied to translation, question answering, reasoning, code generation, and even multimodal understanding and generation, thereby opening unprecedented prospects for the development of general artificial intelligence.

### 2.2. Autoregression in Visual Generation.

Autoregression has been explored in the field of visual generation for many years. Early pixel-based methods [7, 29] applied raster-scan order to directly convert two-dimensional images into one-dimensional pixel sequences for pixel-by-pixel prediction. This paradigm is inefficient in generation and often produces suboptimal and blurry results due to the inherent redundancy of pixel information.

The advent of token-based models marked a major breakthrough in visual autoregressive modeling, inspired by natural language processing (NLP) [3]. Unlike pixel-level models that directly handle raw visual data, this paradigm first compresses visual data into compact token sequences via discrete tokenizers [11, 36, 45], and quantizes them to the nearest codes in a fixed-size codebook to form compact token sequences. It then autoregressively predicts these tokens in raster scan order [17, 26, 44]. However, the improvement in efficiency is still limited. Autoregressive visual generative models trained with a next-token prediction targets require  $n^2$  sequential model forward passes to generate an image represented by  $n \times n$  tokens, leading to a significant reduction in generation efficiency. This issue is particularly prominent in high-resolution image [4] or video generation [14, 35], hindering their widespread application in real-world applications. To accelerate sequence generation, researchers explore the parallel prediction methods. Parallel prediction can generally be divided into two categories: raster-scan order and random-scan order. Among them, parallel prediction in raster-scan order targets a set of spatially regular tokens [12, 39]. Random-scan order is first proposed by MaskGIT [6], which employs a masked generation approach to generate next token set instead of next one token, substantially reducing the inference steps. However, when the number of inference steps is small, the generation quality of both types of efficient autoregressive methods becomes suboptimal. VAR is the first to break the limitation of inference steps on generation performance. By developing coarse-to-fine next-scale predictions, it transitions visual autoregressive modeling from the token level to the scale level, completing the generation process with only 10 steps. However, VAR relies on a multi-scale VQ-GAN [17, 27] that is tightly integrated with the generator and has been trained across a series of complex scales. Furthermore, the VAR generator is constrained by its complex and rigid multi-scale architecture. Modifying the output resolution or adjusting inference steps requires retraining both the tokenizer and generator, resulting in poor scalabil-

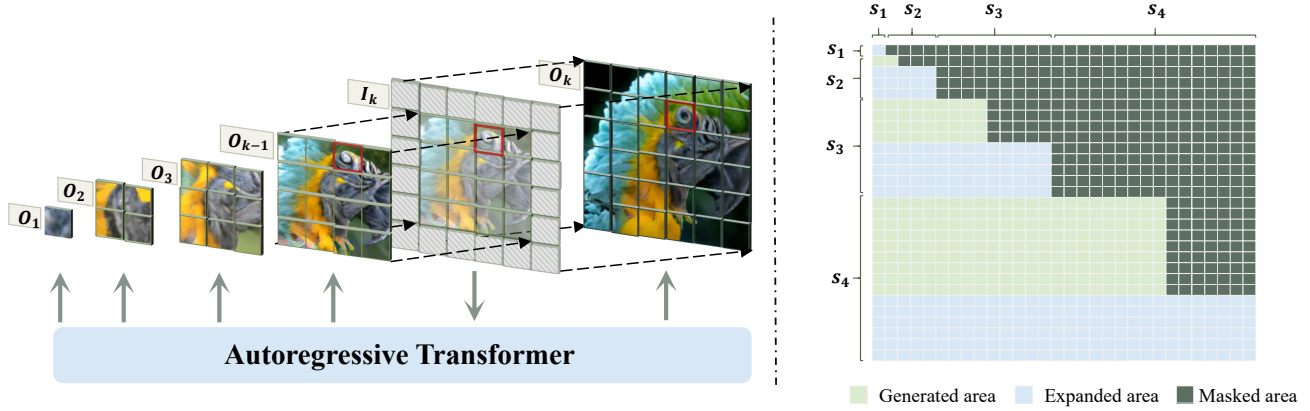


Figure 3. Illustration of our radial-parallel autoregressive (RadAR) generation framework. (a) **Model implementation.** RadAR takes the output  $O_{k-1}$  from step  $k-1$  and then uses learnable parameters to fill the range to be expanded outside  $O_{k-1}$ , forming the input  $I_k$  for step  $k$ . For specific details on the extrapolation range, please refer to Algorithm 1. (b) **Nested attention mask.** For step  $k$ , green corresponds to the range where content has already been generated, and blue corresponds to the new unknown area expanded. The attention range is restricted to distinguish between the two purposes of error correction and content generation. Specifically, the newly expanded area in step  $k$  accesses the context information of all tokens from previous  $k-1$  steps and step  $k$  to complete the generation purpose, while the generated area is restrict from accessing the expanded area.

ity. Additionally, its specialized multi-scale tokenizer creates compatibility barriers when integrating with large language models for multimodal unification, significantly limiting flexibility.

### 3. Method

**Radial-Parallel Autoregressive Modeling.** Our proposed parallel autoregressive method is illustrated in Fig. 3. Unlike the common raster order, the generation process is concentric, akin to progressively adding borders from the center to the surroundings, starting from scratch. At step  $t$ , the model receives the already generated rectangular area and adds a border of a certain thickness around it. This border is filled with a learnable prompt vector  $p \in R^{c \times 1 \times 1}$ , and then the generated area along with the prompt is processed as the input for the current step. This concentric stacking mechanism enables highly parallel expansion while maintaining strong spatial locality through radial dependencies. In the specific implementation, we first perform center cropping on the quantized latent feature  $f_q$  to obtain  $N$  token sets  $\{g_1, g_2, \dots, g_N\}$  with incrementally larger spatial ranges, where  $g_k = \{x_i\}_{i=0}^n$ . The spatial range represented by these token sets increases progressively, with the final  $g_N$  matching the range of the original feature map  $R^{c \times h \times w}$ , that is,  $g_N = f_q$ . Algorithm 1 provides a detailed description of the data preprocessing before autoregressive training. The autoregressive likelihood function is reformulated as:

$$p(g_1, g_2, \dots, g_N) = \prod_{i=1}^N p(g_i | g_1, g_2, \dots, g_{i-1}). \quad (1)$$

Crucially, our method enables dynamic context updating, allowing each generation step to optimize previously synthesized areas using the latest context information, thereby implementing an implicit error correction mechanism. This mitigates the accumulation of prediction errors common in parallel token generation, achieving an optimal balance between parallelization efficiency (allowing concurrent generation of spatially independent border segments) and maintenance of generation quality. As a result, compared to traditional parallel autoregressive methods, the number of decoding steps required is significantly reduced while avoiding their characteristic error propagation issues.

**Nested Attention Mechanism.** To address the distinct objectives of the already generated area, which requires minor corrections for potential generation errors, and the newly expanded area, which necessitates generating content from scratch, we introduce the nested attention mechanism as illustrated in Fig. 3. Specifically, causal attention is applied between steps to ensure the orderly progression of the autoregressive process, while bidirectional attention is employed within each step to maintain spatial consistency. Moreover, to prevent the error-prone newly expanded area from misleading the error correction decisions of the already generated area, causal attention is also maintained between the known and newly expanded areas within each step. During inference, KV-caching is used and no mask is needed. The experimental section compares the effects of using and not using this nested attention mechanism.

**Tokenizer Post-training.** To mitigate the gap between the latent space sampled by the generator and the latent space seen during tokenizer training, we introduced a



Figure 4. Visualization of error correction. Earlier generation errors are gradually corrected by the subsequent generation process as the number of inference steps increases. Please zoom in for details.

---

### Algorithm 1 Radial-Parallel Autoregressive Encoding

---

**Input:** raw image  $im$ , learnable vector  $p$

**Parameter:** steps  $N$ , current patch nums  $\{P_i\}_{i=1}^N$

**Output:** regression input token sets  $R_s$  and regression target token sets  $R_{gt}$

```

1:  $f = \mathcal{E}(im)$ 
2:  $f_q = \mathcal{Q}(f)$ 
3:  $i = 1$ 
4: while  $i < N + 1$  do
5:    $g_i = \text{crop}(f_q, P_i)$ 
6:    $R_{gt} = \text{queue\_push}(R_{gt}, g_i)$ 
7:   if  $i < N$  then
8:      $S_{i+1} = \text{repeat}(p, P_{i+1})$ 
9:      $S_{i+1} = \text{center\_fill}(S_{i+1}, g_i, P_i, P_{i+1})$ 
10:     $R_s = \text{queue\_push}(R_s, S_{i+1})$ 
11:   end if
12: end while

```

---

lightweight post-training phase. Deviating from the standard teacher-forcing technique, the input for the next autoregressive step is a composite of the output from the previous autoregressive step and the ground-truth, amalgamated in a specified ratio. The loss function is composed of two parts and is represented as:

$$L_{vqgan} = L_{recon} + L_{GAN} + L_{percp} + L_{vq},$$

$$L = \frac{\lambda}{N} \sum_{n=1}^N \cos(f_n^{dec,l}, \phi(f_n^{DINO})) + L_{vqgan}. \quad (2)$$

where  $L_{vqgan}$  includes  $L_{recon}$  (the reconstruction loss),  $L_{percp}$  (the perceptual loss),  $L_{GAN}$  (the adversarial loss), and  $L_{vq}$  (the codebook loss). To enable the tokenizer to generate latent representations with greater semantic consistency, we introduce the semantic regularization loss. Here,

$N$  denotes the batch size, and  $n$  represents the image index. An MLP is used to project the decoder feature  $f_n^{dec,l}$  to match the channel dimension of the feature from a pre-trained visual encoder (here DINOv2-B). The semantic regularization loss aligns the features by computing the cosine similarity, thereby constraining the complexity of the latent space and preventing the tokenizer from learning overly complex latent dependencies.

## 4. Experiments

In this section, we first introduce the experimental setup, including datasets, metrics, baselines, and implementation details. Then, we compare RadAR with state-of-the-art methods, followed by ablation studies to analyze the effectiveness of each component and some zero-shot generation experiments to demonstrate the flexibility of RadAR.

### 4.1. Experimental Settings

**Implementation Details.** Our tokenizer is initialized with the pre-trained weights of llamaGen [31], with the codebook size set to 8912. It downsamples the input image at a fixed ratio of 16×16. We mainly follow the VQVAE training recipe of llamaGen and fine-tune on ImageNet-1K [8] with randomly sampled resolutions. RadAR is also trained on the ImageNet-1K [8] 256×256 dataset. The training process employs the AdamW optimizer [1] with  $\beta_1 = 0.9$ ,  $\beta_2 = 0.95$ , and a weight decay rate of 0.05. The learning rate is set to 1e-4, and the training epochs are uniformly set to 300 epochs.

**Baselines.** We choose baseline methods from popular image generation models, including generative adversarial networks (GAN.) [2, 15, 30], diffusion models(Diff.) [9, 23], masked-prediction models (Mask.) [6, 18, 20], visual autoregressive models (VAR.) [33, 43] and autoregressive models (AR.) [12, 31, 39]. These methods have achieved impressive results on various image generation tasks and

Table 1. Performance comparisons on class-conditional ImageNet 256×256 benchmark. Metrics are Frechet inception distance (FID), inception score (IS), precision and recall. “↓” or “↑” indicate lower or higher values are better. “Steps” denotes the number of model forward passes required to generate an image. MAR (step=10) is evaluated using code and pretrained weights from their official GitHub repository. **Bold** denotes the best, and underline denotes the second.

Type	Model	Params	Steps↓	FID↓	IS↑	Precision↑	Recall↑
GAN	BigGAN [2]	112M	1	6.95	224.5	0.89	0.38
	GigaGAN [15]	569M	1	3.45	225.5	0.84	0.61
	StyleGAN-XL [30]	166M	1	2.30	265.1	0.78	0.53
Diff	ADM-G [9]	554M	250	4.59	186.7	0.82	0.52
	ADM [9]	554M	250	10.94	101.0	0.69	0.63
	DiT-L/2 [22]	458M	250	5.02	167.2	0.75	0.57
	DiT-XL/2 [22]	675M	250	2.27	278.2	0.83	0.57
Mask	MaskGIT [6]	227M	8	6.18	182.1	0.8	0.51
	Open-MAGVIT2 [20]	343M	256	3.08	258.3	0.85	0.51
	MAR-H [18]	943M	10	9.32	207.4	0.71	0.47
VAR	VAR-d16 [33]	310M	10	3.55	280.4	0.84	0.51
	VAR-d20 [33]	600M	10	2.95	302.6	0.83	0.56
	FAR-B [43]	208M	10	4.26	248.9	0.79	0.51
	FAR-H [43]	812M	10	3.21	300.6	0.81	0.55
AR	LlamaGen-L [31]	343M	256	3.80	248.3	0.83	0.52
	LlamaGen-XL [31]	775M	256	3.39	227.1	0.81	0.54
	LlamaGen-XXL [31]	1.4B	256	3.09	253.6	0.83	0.53
Parallelized AR	PAR-L-4× [39]	343M	67	4.32	189.4	<b>0.87</b>	0.43
	PAR-XL-4× [39]	775M	67	3.50	234.4	0.84	0.49
	NAR-L [12]	372M	31	3.06	263.9	0.81	0.53
	NAR-XL [12]	816M	31	<b>2.70</b>	277.5	0.81	<b>0.58</b>
	RadAR	310M	10	3.50	<b>307.9</b>	0.81	0.50
	RadAR	310M	13	3.36	289.5	0.84	<u>0.54</u>
	RadAR	610M	10	3.21	291.4	0.83	<u>0.52</u>
	RadAR	610M	13	<u>2.97</u>	<u>303.8</u>	<u>0.85</u>	0.53

serve as strong baselines for comparison. Since the prediction of our method is token-based and aligns with the objectives of AR methods like LlamaGen [31], we take it as a strong baseline and primarily compare our method with it.

**Evaluation Metrics.** We adopt four metrics for quantitative evaluation: Frechet Inception Distance (FID) [13], Inception Score (IS) [28], Precision, and Recall [16]. Following the standard protocols, we sample 50,000 images with trained models to evaluate.

## 4.2. Class-conditional Image Generation

In this section, we evaluate the performance of RadAR on the ImageNet, with the results shown in Table 1. We provide two scales of RadAR, L and XL. Compared with state-of-the-art models, RadAR shows significant competitiveness in multiple key metrics, including inference steps, FID, IS, precision, and recall. Among AR methods, RadAR significantly reduced the number of inference steps required

for image generation. Specifically, compared with the 256 steps required for the token-by-token generation process of LlamaGen and the 67 steps required for the parallel generation mechanism of PAR, RadAR reduces the number of inference steps to approximately 10. This reduction is not only quantitative but also accompanied by improved generation performance, making RadAR a leading candidate for efficient and high-quality image synthesis. Compared with the multi-scale VAR methods, although the FID and recall scores of RadAR are slightly lower than those of VAR, it achieves higher IS and Precision scores. This indicates that RadAR excels in generating images with higher perceptual quality and more accurate details, although it may sacrifice overall diversity and recall to some extent.

Since RadAR’s prediction target is the ground-truth value, this design brings multiple benefits. On the one hand, RadAR can dynamically adjust the number of inference steps according to the desired generation effect and

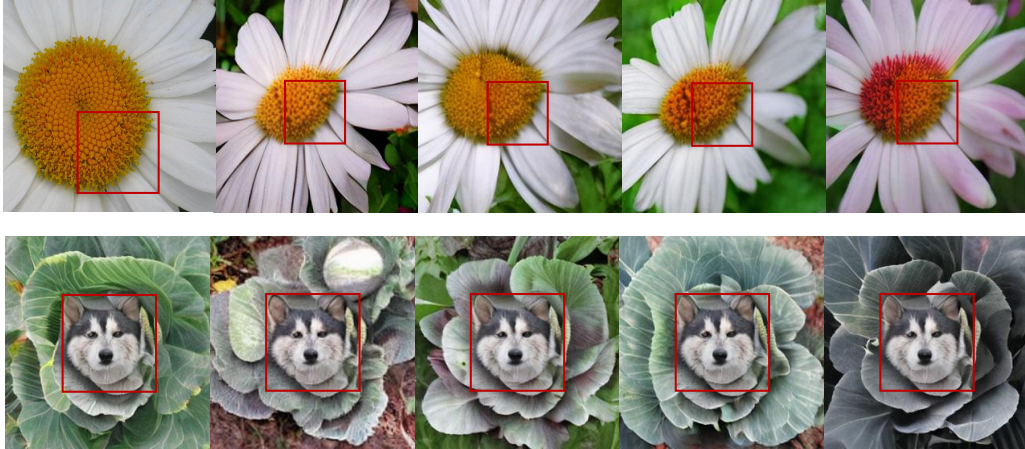


Figure 5. Zero-shot evaluation in downstream tasks containing out-painting and class-conditional editing. The results show that RadAR can generalize to novel downstream tasks without special design and finetuning. Please zoom in for details.

computational efficiency. In contrast, methods that predict residuals, such as VAR, need to retrain the tokenizer and autoregressive generator if the number of inference steps is to be changed. This adaptability highlights RadAR’s strong generalization ability. On the other hand, this modeling approach is highly consistent with the requirements of multimodal vision-language models (VLMs). By directly predicting the ground-truth value, RadAR ensures that the generated images are not only perceptually realistic but also semantically consistent with the input prompts. This seamless integration with VLMs is an advantage that residual modeling methods do not possess. Overall, RadAR achieves a balanced and advanced level in terms of inference efficiency and generation quality, making it a strong competitor in the field of autoregressive visual generation.

### 4.3. Ablation Study

**Component-wise Ablations.** In Table 2, we conduct comprehensive ablation studies to investigate the effectiveness of our key designs on the ImageNet 256×256 dataset. Specifically, these include: 1) Nested Attention Mechanism (NAM): This attention mechanism disentangles the functions of error correction and ground-truth value prediction, thereby improving the FID score. 2) Random Dropout Sampling (RDS): This training sampling strategy not only enhances RadAR’s ability to perceive arbitrary inference ranges but also increases the flexibility of the model’s inference steps. 3) Random Noise Input (RNI): This technique increases the model’s tolerant ability for deviations between generated results and ground-truth during inference, thereby improving the score of IS. 4) Tokenizer Post-training (TPT): This mechanism effectively mitigates the gap between the latent space sampled by the generator and the latent space, resulting in significant improvement of

Table 2. Ablations on the effectiveness of the proposed techniques. Specific meanings of the abbreviations are in the ablation part. We report the results with RadAR-XL.

Ablations				Metrics			
NAM	RDS	RNI	TPT	FID↓	IS↑	Pre↑	Rec↑
×	×	×	×	5.70	255.0	0.81	0.41
✓	×	×	×	3.80	271.0	0.80	0.50
✓	✓	×	×	3.60	295.4	0.80	0.52
✓	✓	✓	×	3.55	297.6	0.80	0.52
✓	✓	✓	✓	3.31	299.4	0.82	0.53

each evaluation metrics.

**Visualization of Error Correction.** Autoregressive parallel generation improves the efficiency of visual generation but also raises the probability of token errors. This is one of the primary reasons why the performance of previous methods drops sharply when the autoregressive steps are highly compressed. Unlike traditional autoregressive methods, RadAR can adaptively detect and correct generation errors in the early stages of inference while generating new tokens. As shown in Fig. 4, as the number of inference steps increases, some minor errors in the early stages are identified and corrected with the help of richer context information. For example, the parrot’s feathers become clearer, and the shapes of the owl’s eyes and beak become more normal.

**Initial Token Position.** To evaluate the influence of initial token positions in the parallel generation, we conduct ablation studies comparing different starting location configurations, with quantitative results presented in Table 3. The experiments demonstrate that initialization from the center position yields superior performance relative to edge-based initialization, which in turn surpasses corner-

Table 3. Ablations on the initial token position (RadAR-XL).

Position	center	edge	corner
FID↓	3.31	3.45	3.51
IS↑	299.4	293.5	288.4

Table 4. Class-conditional image generation speed.

Model	Params	Steps	Throughput↑ (img/s)	IS↑
VAR	310M	10	112.4	280.4
LlamaGen	343M	256	20.3	248.3
PAR	343M	67	41.7	189.4
NAR	372M	31	65.2	263.9
RadAR	310M	10	113.6	307.9

based initialization. This observed hierarchy suggests that the performance advantage is closely associated with the symmetrical propagation of contextual information during inference. Beyond quantitative metrics, the center-token initialization strategy also enables the most balanced high-parallelism computation, as radial expansion originating from the center facilitates uniform distribution of computational load across directional paths. These collective findings support the adoption of center-oriented initialization as the optimal configuration in the RadAR, effectively harmonizing generation quality with computational efficiency.

**Image Generation Speed.** In Table 4, we compare the generation speed of different autoregressive models with similar numbers of parameters on ImageNet  $256 \times 256$ . The results demonstrate that RadAR achieves a maximum speedup of approximately  $5.6\times$  relative to LlamaGen, while achieving generation efficiency comparable to VAR. More notably, RadAR maintains this competitive speed advantage without sacrificing architectural compatibility with mainstream visual token representations. This represents a notable practical advantage over VAR, which necessitates substantial modifications to the token representation architecture to attain similar efficiency improvements, consequently constraining its integration potential with existing multimodal systems. Collectively, these findings indicate that RadAR effectively mitigates the fundamental efficiency limitations of traditional autoregressive models while circumventing the compatibility challenges associated with alternative parallel generation methodologies. The framework establishes an optimal balance between generation speed, output quality, and system integration flexibility, positioning it as a viable solution for practical applications demanding high-throughput visual content synthesis.

#### 4.4. Zero-shot Task Generalization

**Image Out-painting.** We place the ground-truth tokens in

the unmasked area and let the model generate the tokens in the masked area. Fig. 5 (top) shows a set of results from RadAR-XL. Without any fine-tuning, RadAR can successfully complete the outpainting task, with natural transitions at the boundary junctions, demonstrating RadAR’s good generalization ability.

**Class-conditional Image Editing.** Furthermore, RadAR is applied to the class-conditional image editing task. Similar to the outpainting task, we place the ground-truth tokens in the unmasked area. The difference is that we use specific class labels as conditional to guide the generation of tokens in the masked area. The visualization results are shown in Fig. 5 (bottom), where RadAR can naturally blend images from different categories, once again demonstrating its powerful generation capability.

**Generate Images at high Resolution.** In Fig. 6, we visualize the result of zero-shot generation at high-resolution. We take low-resolution images as the input, and RadAR can generate high quality high-resolution images. Compared to VAR [33], which requires retraining the tokenizer and Autoregressive generator completely, our RadAR, despite being trained only at the  $256 \times 256$  resolution, can accomplish this task without fine-tuning, thanks to its inherent capability of both generation and refinement.

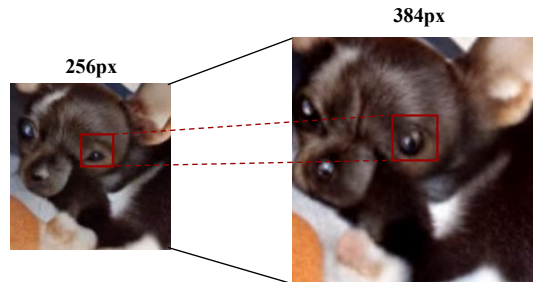


Figure 6. Visualization of Generation at high resolution. RadAR-XL (trained at 256px) is used. Zoom in for details.

## 5. Conclusion

In this paper, we introduce RadAR, which aims to address the limitations of traditional autoregressive models in terms of efficiency and flexibility. RadAR employs a unique inside-out, radial-parallel decoding strategy that ensures spatial consistency. Moreover, RadAR can dynamically correct existing generation errors during the inference process, thereby significantly reducing the number of inference steps required for image generation while maintaining high visual quality. Additionally, RadAR demonstrates strong generalization ability by successfully completing zero-shot image-to-image generation tasks and generating images with various aspect ratios, showing its competitiveness in the field of autoregressive visual generation.

## References

- [1] Kingma DP Ba J Adam et al. A method for stochastic optimization. *arXiv preprint arXiv:1412.6980*, 1412(6), 2014. 5
- [2] Andrew Brock, Jeff Donahue, and Karen Simonyan. Large scale gan training for high fidelity natural image synthesis. In *International Conference on Learning Representations*, 2018. 5, 6
- [3] Tom Brown, Benjamin Mann, Nick Ryder, Melanie Subbiah, Jared D Kaplan, Prafulla Dhariwal, Arvind Neelakantan, Pranav Shyam, Girish Sastry, Amanda Askell, et al. Language models are few-shot learners. *Advances in neural information processing systems*, 33:1877–1901, 2020. 2, 3
- [4] Shiyue Cao, Yueqin Yin, Lianghua Huang, Yu Liu, Xin Zhao, Deli Zhao, and Kaigi Huang. Efficient-vqgan: Towards high-resolution image generation with efficient vision transformers. In *Proceedings of the IEEE/CVF International Conference on Computer Vision*, pages 7368–7377, 2023. 3
- [5] Mathilde Caron, Hugo Touvron, Ishan Misra, Hervé Jégou, Julien Mairal, Piotr Bojanowski, and Armand Joulin. Emerging properties in self-supervised vision transformers. In *Proceedings of the IEEE/CVF international conference on computer vision*, pages 9650–9660, 2021. 2
- [6] Huiwen Chang, Han Zhang, Lu Jiang, Ce Liu, and William T Freeman. Maskgit: Masked generative image transformer. In *Proceedings of the IEEE/CVF conference on computer vision and pattern recognition*, pages 11315–11325, 2022. 2, 3, 5, 6
- [7] Van den Oord. Conditional image generation with pixelcnn decoders. *Adv. Neural Inf. Process. Syst.*, 29, 2016. 3
- [8] Jia Deng, Wei Dong, Richard Socher, Li-Jia Li, Kai Li, and Li Fei-Fei. Imagenet: A large-scale hierarchical image database. In *2009 IEEE conference on computer vision and pattern recognition*, pages 248–255. Ieee, 2009. 5
- [9] Prafulla Dhariwal and Alexander Nichol. Diffusion models beat gans on image synthesis. *Advances in neural information processing systems*, 34:8780–8794, 2021. 5, 6
- [10] Abhimanyu Dubey, Abhinav Jauhri, Abhinav Pandey, Abhishek Kadian, Ahmad Al-Dahle, Aiesha Letman, Akhil Mathur, Alan Schelten, Amy Yang, Angela Fan, et al. The llama 3 herd of models. *arXiv e-prints*, pages arXiv–2407, 2024. 2
- [11] Patrick Esser, Robin Rombach, and Bjorn Ommer. Taming transformers for high-resolution image synthesis. In *Proceedings of the IEEE/CVF conference on computer vision and pattern recognition*, pages 12873–12883, 2021. 2, 3
- [12] Yefei He, Yuanyu He, Shaoxuan He, Feng Chen, Hong Zhou, Kaipeng Zhang, and Bohan Zhuang. Neighboring autoregressive modeling for efficient visual generation. *arXiv preprint arXiv:2503.10696*, 2025. 3, 5, 6
- [13] Martin Heusel, Hubert Ramsauer, Thomas Unterthiner, Bernhard Nessler, and Sepp Hochreiter. Gans trained by a two time-scale update rule converge to a local nash equilibrium. *Advances in neural information processing systems*, 30, 2017. 6
- [14] Wenyi Hong, Ming Ding, Wendi Zheng, Xinghan Liu, and Jie Tang. Cogvideo: Large-scale pretraining for text-to-video generation via transformers. *arXiv preprint arXiv:2205.15868*, 2022. 3
- [15] Minguk Kang, Jun-Yan Zhu, Richard Zhang, Jaesik Park, Eli Shechtman, Sylvain Paris, and Taesung Park. Scaling up gans for text-to-image synthesis. In *Proceedings of the IEEE/CVF conference on computer vision and pattern recognition*, pages 10124–10134, 2023. 5, 6
- [16] Tuomas Kynkäänniemi, Tero Karras, Samuli Laine, Jaakko Lehtinen, and Timo Aila. Improved precision and recall metric for assessing generative models. *Advances in neural information processing systems*, 32, 2019. 6
- [17] Doyup Lee, Chiheon Kim, Saehoon Kim, Minsu Cho, and Wook-Shin Han. Autoregressive image generation using residual quantization. In *Proceedings of the IEEE/CVF conference on computer vision and pattern recognition*, pages 11523–11532, 2022. 3
- [18] Tianhong Li, Yonglong Tian, He Li, Mingyang Deng, and Kaiming He. Autoregressive image generation without vector quantization. *Advances in Neural Information Processing Systems*, 37:56424–56445, 2024. 5, 6
- [19] Aixin Liu, Bei Feng, Bing Xue, Bingxuan Wang, Bochao Wu, Chengda Lu, Chenggang Zhao, Chengqi Deng, Chenyu Zhang, Chong Ruan, et al. Deepseek-v3 technical report. *arXiv preprint arXiv:2412.19437*, 2024. 2
- [20] Zhuoyan Luo, Fengyuan Shi, Yixiao Ge, Yujiu Yang, Limin Wang, and Ying Shan. Open-magvit2: An open-source project toward democratizing auto-regressive visual generation. *arXiv preprint arXiv:2409.04410*, 2024. 5, 6
- [21] Maxime Oquab, Timothée Darcet, Théo Moutakanni, Huy Vo, Marc Szafraniec, Vasil Khalidov, Pierre Fernandez, Daniel Haziza, Francisco Massa, Alaaeldin El-Nouby, et al. Dinov2: Learning robust visual features without supervision. *arXiv preprint arXiv:2304.07193*, 2023. 2
- [22] William Peebles and Saining Xie. Scalable diffusion models with transformers. In *Proceedings of the IEEE/CVF international conference on computer vision*, pages 4195–4205, 2023. 6
- [23] Alec Radford, Karthik Narasimhan, Tim Salimans, Ilya Sutskever, et al. Improving language understanding by generative pre-training. 2018. 5
- [24] Alec Radford, Jeffrey Wu, Rewon Child, David Luan, Dario Amodei, Ilya Sutskever, et al. Language models are unsupervised multitask learners. *OpenAI blog*, 1(8):9, 2019. 3
- [25] Alec Radford, Jong Wook Kim, Chris Hallacy, Aditya Ramesh, Gabriel Goh, Sandhini Agarwal, Girish Sastry, Amanda Askell, Pamela Mishkin, Jack Clark, et al. Learning transferable visual models from natural language supervision. In *International conference on machine learning*, pages 8748–8763. Pmlr, 2021. 2
- [26] Aditya Ramesh, Mikhail Pavlov, Gabriel Goh, Scott Gray, Chelsea Voss, Alec Radford, Mark Chen, and Ilya Sutskever. Zero-shot text-to-image generation. In *International conference on machine learning*, pages 8821–8831. Pmlr, 2021. 2, 3
- [27] Ali Razavi, Aaron Van den Oord, and Oriol Vinyals. Generating diverse high-fidelity images with vq-vae-2. *Advances in neural information processing systems*, 32, 2019. 2, 3

- [28] Tim Salimans, Ian Goodfellow, Wojciech Zaremba, Vicki Cheung, Alec Radford, and Xi Chen. Improved techniques for training gans. *Advances in neural information processing systems*, 29, 2016. 6
- [29] Tim Salimans, Andrej Karpathy, Xi Chen, and Diederik P Kingma. Pixelcnn++: Improving the pixelcnn with discretized logistic mixture likelihood and other modifications. *arXiv preprint arXiv:1701.05517*, 2017. 3
- [30] Axel Sauer, Katja Schwarz, and Andreas Geiger. Stylegan-xl: Scaling stylegan to large diverse datasets. In *ACM SIGGRAPH 2022 conference proceedings*, pages 1–10, 2022. 5, 6
- [31] Peize Sun, Yi Jiang, Shoufa Chen, Shilong Zhang, Bingyue Peng, Ping Luo, and Zehuan Yuan. Autoregressive model beats diffusion: Llama for scalable image generation. *arXiv preprint arXiv:2406.06525*, 2024. 2, 3, 5, 6
- [32] Chameleon Team. Chameleon: Mixed-modal early-fusion foundation models, 2024. URL <https://arxiv.org/abs/2405.09818>, 9(8), 2024. 2
- [33] Keyu Tian, Yi Jiang, Zehuan Yuan, Bingyue Peng, and Liwei Wang. Visual autoregressive modeling: Scalable image generation via next-scale prediction. *Advances in neural information processing systems*, 37:84839–84865, 2024. 2, 5, 6, 8
- [34] Shengbang Tong, David Fan, Jiachen Li, Yunyang Xiong, Xinlei Chen, Koustuv Sinha, Michael Rabbat, Yann LeCun, Saining Xie, and Zhuang Liu. Metamorph: Multimodal understanding and generation via instruction tuning. In *Proceedings of the IEEE/CVF International Conference on Computer Vision*, pages 17001–17012, 2025. 2
- [35] Sergey Tulyakov, Ming-Yu Liu, Xiaodong Yang, and Jan Kautz. Mocogan: Decomposing motion and content for video generation. In *Proceedings of the IEEE conference on computer vision and pattern recognition*, pages 1526–1535, 2018. 3
- [36] Aaron Van Den Oord, Oriol Vinyals, et al. Neural discrete representation learning. *Advances in neural information processing systems*, 30, 2017. 3
- [37] Ashish Vaswani, Noam Shazeer, Niki Parmar, Jakob Uszkoreit, Llion Jones, Aidan N Gomez, Łukasz Kaiser, and Illia Polosukhin. Attention is all you need. In *Proceedings of the 31st International Conference on Neural Information Processing Systems*, page 6000–6010, 2017. 3
- [38] Zhongwei Wan, Xin Wang, Che Liu, Samiul Alam, Yu Zheng, Jiachen Liu, Zhongnan Qu, Shen Yan, Yi Zhu, Quanlu Zhang, et al. Efficient large language models: A survey. *arXiv preprint arXiv:2312.03863*, 2023. 3
- [39] Yuqing Wang, Shuhuai Ren, Zhijie Lin, Yujin Han, Haoyuan Guo, Zhenheng Yang, Difan Zou, Jiashi Feng, and Xihui Liu. Parallelized autoregressive visual generation. In *Proceedings of the Computer Vision and Pattern Recognition Conference*, pages 12955–12965, 2025. 2, 3, 5, 6
- [40] Yecheng Wu, Zhuoyang Zhang, Junyu Chen, Haotian Tang, Dacheng Li, Yunhao Fang, Ligeng Zhu, Enze Xie, Hongxu Yin, Li Yi, et al. Vila-u: a unified foundation model integrating visual understanding and generation. *arXiv preprint arXiv:2409.04429*, 2024. 2
- [41] Jinheng Xie, Weijia Mao, Zechen Bai, David Junhao Zhang, Weihao Wang, Kevin Qinghong Lin, Yuchao Gu, Zhijie Chen, Zhenheng Yang, and Mike Zheng Shou. Show-o: One single transformer to unify multimodal understanding and generation. *arXiv preprint arXiv:2408.12528*, 2024. 2
- [42] An Yang, Anfeng Li, Baosong Yang, Beichen Zhang, Binyuan Hui, Bo Zheng, Bowen Yu, Chang Gao, Chengen Huang, Chenxu Lv, et al. Qwen3 technical report. *arXiv preprint arXiv:2505.09388*, 2025. 2
- [43] Hu Yu, Hao Luo, Hangjie Yuan, Yu Rong, and Feng Zhao. Frequency autoregressive image generation with continuous tokens. *arXiv preprint arXiv:2503.05305*, 2025. 5, 6
- [44] Jiahui Yu, Yuanzhong Xu, Jing Yu Koh, Thang Luong, Gungjan Baid, Zirui Wang, Vijay Vasudevan, Alexander Ku, Yinfei Yang, Burcu Karagol Ayan, et al. Scaling autoregressive models for content-rich text-to-image generation. *arXiv preprint arXiv:2206.10789*, 2(3):5, 2022. 2, 3
- [45] Lijun Yu, José Lezama, Nitesh B Gundavarapu, Luca Versari, Kihyuk Sohn, David Minnen, Yong Cheng, Vignesh Birodkar, Agrim Gupta, Xiuye Gu, et al. Language model beats diffusion–tokenizer is key to visual generation. *arXiv preprint arXiv:2310.05737*, 2023. 3
- [46] Xiaohua Zhai, Basil Mustafa, Alexander Kolesnikov, and Lucas Beyer. Sigmoid loss for language image pre-training. In *Proceedings of the IEEE/CVF international conference on computer vision*, pages 11975–11986, 2023. 2
- [47] Yue Zhao, Fuzhao Xue, Scott Reed, Linxi Fan, Yuke Zhu, Jan Kautz, Zhiding Yu, Philipp Krähenbühl, and De-An Huang. Qlip: Text-aligned visual tokenization unifies autoregressive multimodal understanding and generation. *arXiv preprint arXiv:2502.05178*, 2025. 2
- [48] Hongjian Zhou, Fenglin Liu, Boyang Gu, Xinyu Zou, Jinfa Huang, Jinge Wu, Yiru Li, Sam S Chen, Peilin Zhou, Junling Liu, et al. A survey of large language models in medicine: Progress, application, and challenge. *arXiv preprint arXiv:2311.05112*, 2023. 3